Magnetic Linear Dichroism in the Angular Dependence of Core-Level Photoemission from (Ga,Mn)As Using Hard X Rays

K. W. Edmonds,[1] G. van der Laan,[2] N. R. S. Farley,[1] R. P. Campion,[1] B. L. Gallagher,[1] C. T. Foxon,[1] B. C. C. Cowie,[3] S. Warren,[4] and T. K. Johal[4]

[1]*School of Physics and Astronomy, University of Nottingham, Nottingham NG7 2RD, United Kingdom*
[2]*Diamond Light Source, Chilton, Didcot OX11 0DE, United Kingdom*
[3]*European Synchrotron Radiation Facility, 6 rue Jules Horowitz, B.P. 220, F-38043 Grenoble Cedex, France*
[4]*Daresbury Laboratory, Warrington WA4 4AD, United Kingdom*

(Received 8 August 2011; published 1 November 2011)

We report a study of the electronic properties of the ferromagnetic semiconductor (Ga,Mn)As using magnetic linear dichroism in the angular dependence of Mn $2p$ photoemission under hard x-ray excitation. Bulk plasmon loss satellites demonstrate that the probed Mn ions are incorporated deep within the GaAs lattice, while the observed large dichroism indicates that the spectra originate from ferromagnetic substitutional Mn. Simulations of the spectra using an Anderson impurity model show that the ferromagnetic Mn $3d$ electrons of substitutional Mn in (Ga,Mn)As are intermediate between localized and delocalized.

DOI: 10.1103/PhysRevLett.107.197601 PACS numbers: 79.60.Bm, 75.50.Pp, 75.70.−i

Ferromagnetism in the diluted magnetic semiconductor $Ga_{1-x}Mn_xAs$ has attracted considerable interest. The Mn substitutional acceptor provides charge carriers (holes) and also has a partially filled d-electron band with a net magnetic moment. In order to achieve ferromagnetic ordering, it is necessary to dope to concentrations $x \gtrsim 1\%$, an order of magnitude larger than the equilibrium solubility, necessitating an off-equilibrium growth technique such as low-temperature molecular beam epitaxy [1]. As a consequence, it is extremely challenging to obtain a clean, ordered, and defect-free surface. Moreover, at high concentrations Mn is incorporated on both substitutional acceptor and interstitial donor sites [2]. These problems have inhibited a clear understanding of the material properties of $Ga_{1-x}Mn_xAs$. Core-level [3] and valence band [4] x-ray photoemission spectroscopy (PES) have been performed in order to study the local density of states and p-d hybridization, but it remains to be seen whether the states probed in these studies are really representative of substitutional Mn in ferromagnetic $Ga_{1-x}Mn_xAs$ [5,6].

In core-level PES, a core electron is excited into a continuum state which has no interaction with the atom left behind. The core hole with its attractive Coulomb potential can be used as an internal probe to study the electronic response of the local valence electrons. Hard x-ray PES (HAXPES) has recently emerged as an important extension of this technique, offering a more bulk-sensitive probe due to the much longer photoelectron mean free path (typically 2–10 nm) compared to the more commonly used soft x-ray or ultraviolet excitation. This has enabled, e.g., the nondestructive analysis of buried layers and interfaces [7], and the discrimination of bulk and surface related features [8]. Furthermore, using polarized x rays, it is possible to measure the magnetic dichroism in HAXPES in order to probe the magnetic properties [9]. HAXPES studies of $Ga_{1-x}Mn_xAs$ have indicated the importance of Mn diffusion and surface buildup during low-temperature annealing, resulting in a core-level photoemission spectrum dominated by surface oxides even at high energies [10]. More recently, signatures of both substitutional and interstitial Mn were reported in Mn $2p$ HAXPES and photoelectron diffraction studies of $Ga_{1-x}Mn_xAs$ [11]. However, the interpretation of these signatures, and their implications for the electronic structure, require detailed experiments and calculations using, e.g., Anderson impurity model calculations [12].

Here, we present a study of Mn $2p$ core-level PES from $Ga_{1-x}Mn_xAs$ using hard x rays. We observe a clear signature of Mn in bulklike substitutional sites, including the appearance of bulk plasmon loss features as well as a strong magnetic linear dichroism in the angular dependence of photoemission (MLDAD) which uniquely probes the ferromagnetic sites [13].

The PES intensity is a product of photon energy, geometric, and radial dependent terms [14]. MLDAD requires a chiral geometry of the three unit vectors $\hat{\mathbf{P}}$, $\hat{\mathbf{M}}$, and $\hat{\mathbf{k}}$ for the linear polarization, magnetization direction, and photoelectron emission direction, respectively [15,16]. When these vectors are neither coplanar nor mutually perpendicular, reversal of (the odd vector) $\hat{\mathbf{M}}$ results in a geometry with opposite handedness. The chiral geometry is shown in the inset of Fig. 1. By using the handedness of the photoemission experiment, one is able to measure with linear polarization the same dichroism as with circularly polarized x rays in collinear geometry. Charge contributions disappear in the difference spectrum (the MLDAD) and the remaining term is due to the interference of the outgoing $\varepsilon = \ell \pm 1$ continuum states excited from the ℓ

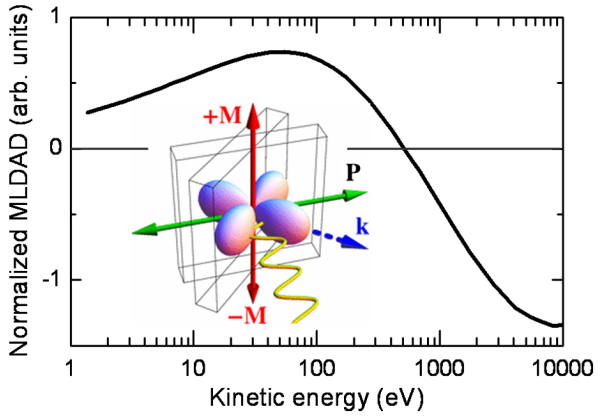

FIG. 1 (color online). Kinetic energy dependence of the normalized MLDAD for Mn $2p$ PES, which is proportional to $R_{2p,\varepsilon s}R_{2p,\varepsilon d}\sin(\delta_{\varepsilon s}-\delta_{\varepsilon d})/(|R_{2p,\varepsilon s}|^2+2|R_{2p,\varepsilon d}|^2)$. The inset gives the chiral geometry for $\hat{\mathbf{M}}$, $\hat{\mathbf{P}}$, and $\hat{\mathbf{k}}$ used in the MLDAD experiment showing two different sample positions. Also shown is the MLDAD angular distribution, which is proportional to $\sin^2\theta\sin 2\phi$ when $\pm\hat{\mathbf{M}} \parallel z$, $\hat{\mathbf{P}} \parallel x$, and $\hat{\mathbf{k}}(\theta, \phi)$. In the experiment, $\theta = 90°$ and $\phi = 45°$.

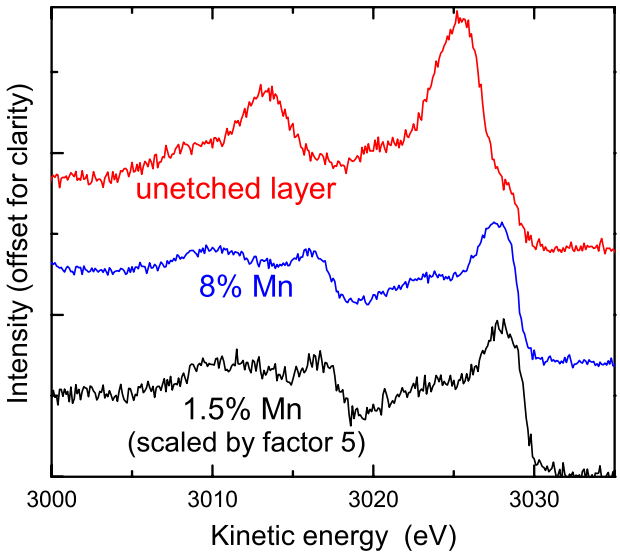

FIG. 2 (color online). Mn $2p$ HAXPES spectra for two etched $Ga_{1-x}Mn_xAs$ films with $x = 1.5\%$ and 8% and for the $x = 8\%$ film prior to etching. The measurements are taken at room temperature using a photon energy of 3670 eV.

core shell. The photon-energy dependent part of the MLDAD signal is proportional to the orbital polarization of the created core hole. This polarized core hole has electrostatic (Coulomb and exchange) interactions with the valence electrons. In contrast to x-ray magnetic circular dichroism (XMCD) in x-ray absorption, where the core electrons are directly excited to $3d$ states, for core-level PES there will be no $3d$ orbital selectivity, and the spectral shape of the MLDAD is independent of the measurement geometry. However, the created core hole provokes a strong screening of the valence electrons, which in the case of MLDAD is strongly spin dependent, resulting in sensitivity to the $3d$ electron localization at ferromagnetic sites.

The angular dependence is proportional to the scalar vector product $\hat{\mathbf{P}}\cdot(\hat{\mathbf{k}}\times\hat{\mathbf{M}})(\hat{\mathbf{P}}\cdot\hat{\mathbf{k}})$, which is plotted in the inset to Fig. 1 [16]. The radial part of the electric-dipole transition probability is proportional to $R_{\ell,\ell-1}R_{\ell,\ell+1}\sin(\delta_{\ell-1}-\delta_{\ell+1})$, where $R_{\ell,\ell\pm1}$ are the radial matrix elements and $\delta_{\ell\pm1}$ the phases of the outgoing $\varepsilon = \ell \pm 1$ continuum states. The calculated kinetic energy dependence of the MLDAD signal for Mn $2p$ PES is plotted in Fig. 1. The signal crosses zero around 500 eV due to the disappearance of the phase difference between outgoing waves, but then reverses sign and strongly gains in magnitude for kinetic energies in the keV range. Therefore, a high x-ray energy is strongly favorable for the measurement of MLDAD, and enables the capture of bulk magnetic properties. Furthermore, the high kinetic energy ensures that the outgoing electron has no interaction with the atom left behind, an important condition for accurate model calculations.

The $Ga_{1-x}Mn_xAs$ films were grown by low-temperature (200–270 °C) molecular beam epitaxy on GaAs(001) substrates. Films of thickness from 10 to 50 nm and Mn concentration x from 1.5% to 8% (estimated from the incident flux rates) were studied. After growth, the films were annealed in air at 190 °C for several hours in order to remove interstitial Mn defects from the lattice. To remove the resulting Mn-rich surface oxides, the film surfaces were etched in concentrated HCl and rinsed in deionized water just prior to mounting the samples in the HAXPES chamber [17].

The HAXPES measurements were performed on beam line ID32 at the European Synchrotron Radiation Facility, Grenoble [18], using linearly polarized hard x rays. The photon energy used was 3670 eV for the PES measurements at room temperature (Figs. 2 and 3), and 4385 eV for the PES and MLDAD measurements at low temperature (Fig. 4) corresponding to a photoelectron attenuation length for Mn $2p$ emission of 3–4 nm [19]. The emitted electrons were collected in a hemispherical electron energy analyzer at an angle of 45° with respect to the x-ray incidence direction. The sample was aligned either at normal x-ray incidence (emission at 45° to sample plane) or normal emission (x-ray incidence at 45° to sample plane). For the MLDAD measurements, the sample was magnetized *in situ* along its in-plane uniaxial easy magnetic axis, using Helmholtz coils attached through an ultra-high vacuum feedthrough to a pulsed current power supply. The magnetization direction was perpendicular to the plane containing the x-ray linear polarization vector and the photoelectron emission direction (see inset to Fig. 1).

Figure 2 compares Mn $2p$ photoemission spectra taken at a photon energy of 3670 eV for two $Ga_{1-x}Mn_xAs$ films with $x = 1.5\%$ and 8%, as well as for the same 8% doped film before HCl etching. Aside from an expected

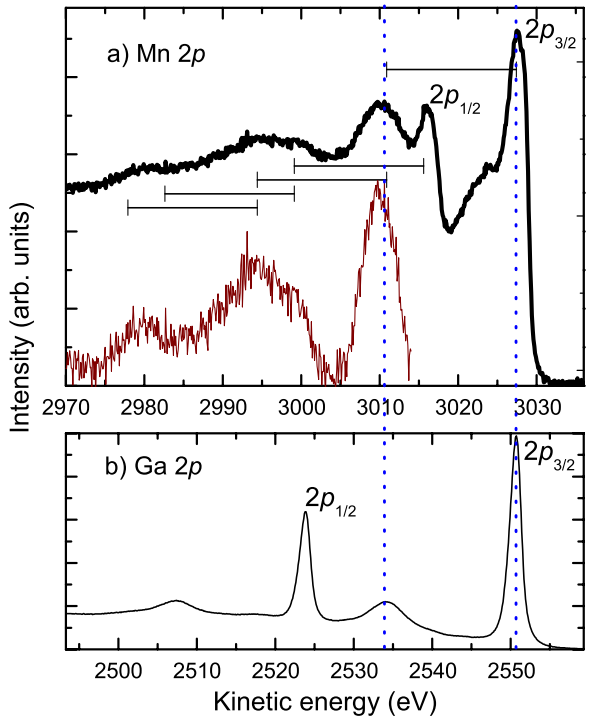

FIG. 3 (color online). (a) Mn $2p$ and (b) Ga $2p$ HAXPES spectra for a $Ga_{0.92}Mn_{0.08}As$ film. The vertical dashed lines locate the positions of the $2p_{3/2}$ photoelectron peak and associated plasmon loss satellite. The horizontal lines span the 16.5 eV characteristic energy loss of the plasmon satellites. The thin line in (a) shows the satellite region of the spectrum after subtracting a linear background and enlarging by a factor of 4. The measurements are taken at room temperature with a photon energy of 3670 eV.

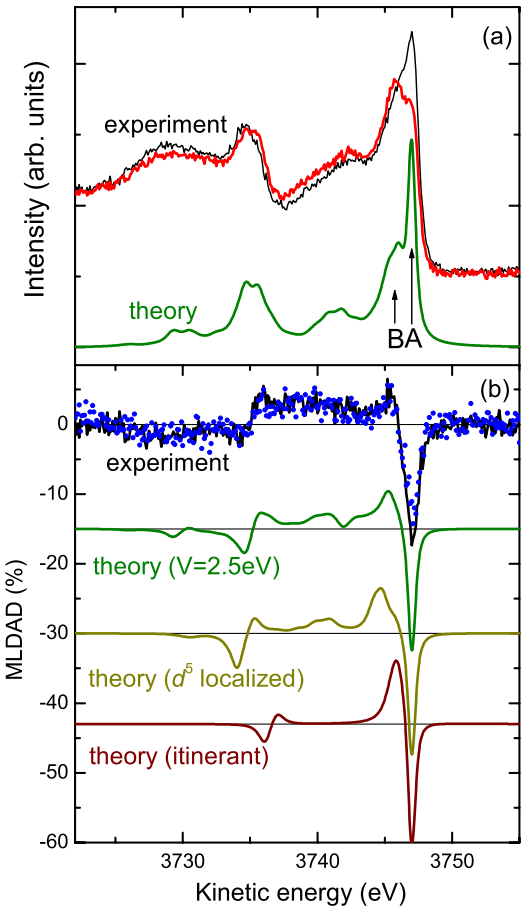

FIG. 4 (color online). Magnetic dichroism in photoemission from (Ga,Mn)As: (a) experimental HAXPES (thin line = +magnetization, thin line = −magnetization) at normal emission, and calculation. The well-screened and poorly screened peak in the $2p_{3/2}$ structure are indicated by A and B, respectively. (b) Experimental MLDAD (points = normal x-ray incidence, line = normal emission), and calculations for an Anderson impurity model with $V = 2.5$ eV, a fully localized d^5 state, and an itinerant electron model. The calculated curves are offset for clarity. The sample temperature is 40 K and the photon energy is 4385 eV.

difference of a factor of ~5 in intensity, the photoemission spectra from the etched films are very similar. In contrast, for the unetched film, the $2p$ photopeaks are shifted to 2 eV lower energy, consistent with previous studies [10,11]. This is due to the oxide layer present on the surface of the unetched film [17].

A number of significant features are visible in the Mn $2p$ spectra from the etched films. The $2p_{3/2}$ spectrum consists of a main peak and a broad satellite at ~4 eV higher binding energy. Such satellite structures are typically observed in core-level PES from transition metal compounds due to multielectron effects. As shown below, the main peak is actually composed of a series of exchange-split peaks corresponding to different final-state electronic configurations. In addition, a large broad peak is observed at 16.5 eV below the $2p_{3/2}$ peak. This peak is a bulk plasmon loss feature, as discussed below.

Figure 3 shows the plasmon loss structures at the Mn $2p$ and Ga $2p$ peaks. Satellites can be observed separated by the characteristic bulk plasmon energy of 16.5 eV from the $2p_{3/2}$ and $2p_{1/2}$ main peaks of both Mn and Ga. Higher-order bulk plasmon satellites associated with the Mn $2p_{3/2}$ peak can also be observed. The observation of such satellites, associated with the excitation of a plasmon within the bulk crystal by the emitted photoelectron, is a strong indication that the measured HAXPES spectrum of the etched film corresponds to Mn incorporated within the GaAs lattice.

To perform the MLDAD measurements, the $x = 8\%$ sample was cooled to 40 K (well below the ferromagnetic transition temperature of ~160 K) and Mn $2p$ spectra were recorded for opposite orientations of the sample magnetization. The resulting spectra are shown in Fig. 4. A sizable difference—the MLDAD signal—is observed, consisting of a sharp negative peak at the lowest binding energy, followed by a smaller positive peak and then a positive plateau up to the $2p_{1/2}$ peak. MLDAD measurements obtained for normal emission (45° x-ray incidence) and

normal incidence (45° electron emission) cf. inset Fig. 1, have the same spectral shape. The MLDAD signal at the $2p_{1/2}$ has reversed sign from the $2p_{3/2}$ peak, due to the core-hole spin-orbit interaction. Because the light interacts only with the orbital part of the wave function, the MLDAD (or MCD) signal is proportional to the core-hole orbital moment [15,16]. Because of the presence of exchange interaction, spin-up states within each core j level will have a higher binding energy than spin-down states. For the $j = 3/2$ levels, the spin and orbital moments of the core hole are coupled parallel, while for the $j = 1/2$ they are coupled antiparallel, leading to the distinctive $(-, +, +, -)$ signature seen in Fig. 4(b).

The photoemission and MLDAD spectra for the transitions $3d^n \rightarrow 2p^5 3d^n \varepsilon$ can be calculated using an Anderson impurity model (AIM) taking into account configuration interaction in initial and final states [12,14]. The wave functions are given as coherent sum over d^n, $d^{n+1}\underline{L}$, $d^{n+2}\underline{L}^2, \ldots$ configurations, where $\underline{L}$ denotes a hole in the ligand orbitals. The average energies of the configurations are taken as points on a parabola, $E(d^n) = n(\Delta - 5U) + \frac{1}{2}n(n-1)U$ and $E(2p^5 d^n) = E(2p^5) + E(d^n) - nQ$, where $\Delta = E(d^6\underline{L}) - E(d^5)$ is the ligand-to-$3d$ charge-transfer energy, U is the $3d$-$3d$ Coulomb energy, and Q is the $2p$-$3d$ Coulomb energy. The configurations are mixed by hybridization with a parameter $V = \langle d|\mathcal{H}|L\rangle$.

The Hamiltonians, $\mathcal{H}$, for the initial and final states of the Mn atoms were calculated using Cowan's code [20], including tetrahedral crystal-field symmetry ($10Dq = -0.5$ eV), spin-orbit and multiplet structure but neglecting band structure dispersion. Wave functions were calculated in intermediate coupling using the atomic Hartree-Fock approximation with relativistic corrections and by reducing the Slater parameters to 80% to account for intra-atomic correlation effects. The plasmon loss satellites were not included in the calculation.

Adopting parameter values similar as for (resonant) PES [3,4,6] and x-ray-absorption spectroscopy [17] of (Ga,Mn)As, a good agreement with the experimental spectra was obtained with $\Delta = 1$ eV, $U = 4$ eV, $Q = 5$ eV, and $V = 2.5$ eV, giving a d count of 5.2 [21]. The AIM calculation is shown in Fig. 4(b), and compared with calculations for an atomic d^5 configuration and an itinerant electron model [16]. The d^5 calculation displays the atomic multiplet structure. When V is turned on, other configurations mix in and the multiplet structure is partly washed out, while a poorly screened peak (marked B in Fig. 4) appears at 1–2 eV higher binding energy. For larger V this poorly screened peak diminishes until it vanishes in the itinerant case. Note that for $V \gg U$ the $3d$ electrons are delocalized, while for $V \ll U$ the electrons remain localized on the atomic sites. The good agreement for intermediate values of V indicates that the Mn $3d$ states are strongly mixed rather than being either purely atomiclike or itinerant.

The simulation reveals that the $2p_{3/2}$ structure is composed of a well-screened peak at the low binding energy side and a poorly screened peak at 1–2 eV higher binding energy, with opposite dichroism. It was previously argued that the splitting of the $2p_{3/2}$ peak is due to the contributions of both substitutional and interstitial Mn to the photoemission spectrum [11]. However, while the PES signal measures all the Mn sites, the MLDAD signal only arises from ferromagnetically ordered Mn. Therefore, the MLDAD measurement and its simulation strongly indicates that the split peaks originate from a single site.

We have presented MLDAD experiments and compared the results to model calculations for the ferromagnetic signal, which was obtained in magnetic remanence. The combination of HAXPES and MLDAD offers an insight into localization and screening of ferromagnetic Mn in (Ga,Mn)As without the complicating effects of the surface. This can have also far reaching implications for the study of other materials. Moreover, we expect that this approach will be widely applicable to a range of complementary experiments including photoelectron diffraction, angle-resolved photoemission, electron holography, and x-ray standing wave studies.

We thank the staff at ESRF for their support during the experiment, and acknowledge funding from EPSRC, STFC, the Royal Society, and the EU (Project No. NAMASTE-214499).

[1] H. Ohno, Science **281**, 951 (1998).
[2] K. M. Yu, W. Walukiewicz, T. Wojtowicz, I. Kuryliszyn, X. Liu, Y. Sasaki, and J. K. Furdyna, Phys. Rev. B **65**, 201303(R) (2002).
[3] J. Okabayashi, A. Kimura, O. Rader, T. Mizokawa, A. Fujimori, T. Hayashi, and M. Tanaka, Phys. Rev. B **58**, R4211 (1998).
[4] J. Okabayashi, A. Kimura, T. Mizokawa, A. Fujimori, T. Hayashi, and M. Tanaka, Phys. Rev. B **59**, R2486 (1999).
[5] H. Asklund, L. Ilver, J. Kanski, J. Sadowski, and R. Mathieu, Phys. Rev. B **66**, 115319 (2002).
[6] O. Rader, C. Pampuch, A. M. Shikin, W. Gudat, J. Okabayashi, T. Mizokawa, A. Fujimori, T. Hayashi, M. Tanaka, A. Tanaka, and A. Kimura, Phys. Rev. B **69**, 075202 (2004).
[7] M. Sing, G. Berner, K. Goss, A. Müller, A. Ruff, A. Wetscherek, S. Thiel, J. Mannhart, S. A. Pauli, C. W. Schneider, P. R. Willmott, M. Gorgoi, F. Schäfers, and R. Claessen, Phys. Rev. Lett. **102**, 176805 (2009).
[8] G. Panaccione, M. Altarelli, A. Fondacaro, A. Georges, S. Huotari, P. Lacovig, A. Lichtenstein, P. Metcalf, G. Monaco, F. Offi, L. Paolasini, A. Poteryaev, O. Tjernberg, and M. Sacchi, Phys. Rev. Lett. **97**, 116401 (2006).
[9] S. Ueda, H. Tanaka, J. Takaobushi, E. Ikenaga, J.-J. Kim, M. Kobata, T. Kawai, H. Osawa, N. Kawamura, M.

Suzuki, and K. Kobayashi, Appl. Phys. Express **1**, 077003 (2008).
[10] B. Schmid, A. Müller, M. Sing, R. Claessen, J. Wenisch, C. Gould, K. Brunner, L. Molenkamp, and W. Drube, Phys. Rev. B **78**, 075319 (2008).
[11] I. Bartos, I. Pis, M. Kobata, K. Kobayashi, M. Cukr, P. Jiricek, T. Sugiyama, and E. Ikenaga, Phys. Rev. B **83**, 235327 (2011).
[12] G. van der Laan and M. Taguchi, Phys. Rev. B **82**, 045114 (2010).
[13] Ch. Roth, F. U. Hillebrecht, H. B. Rose, and E. Kisker, Phys. Rev. Lett. **70**, 3479 (1993).
[14] B. T. Thole and G. van der Laan, Phys. Rev. B **44**, 12424 (1991).
[15] B. T. Thole and G. van der Laan, Phys. Rev. B **49**, 9613 (1994).
[16] G. van der Laan, Phys. Rev. B **51**, 240 (1995); **55**, 3656 (1997).
[17] K. W. Edmonds, N. R. S. Farley, R. P. Campion, C. T. Foxon, B. L. Gallagher, T. K. Johal, G. van der Laan, M. MacKenzie, J. N. Chapman, and E. Arenholz, Appl. Phys. Lett. **84**, 4065 (2004).
[18] J. Zegenhagen, B. Detlefs, T. L. Lee, S. Thiess, H. Isern, L. Petit, L. Andre, J. Roy, Y. Y. Mi, and I. Joumard, J. Electron Spectrosc. Relat. Phenom. **178–179**, 258 (2010).
[19] C. Dallera, L. Duo, L. Braicovich, G. Panaccione, G. Paolicelli, B. Cowie, and J. Zegenhagen, Appl. Phys. Lett. **85**, 4532 (2004).
[20] R. D. Cowan, J. Opt. Soc. Am. **58**, 808 (1968).
[21] The initial-state d weights were 0.3% d^3, 10% d^4, 60.8% d^5, 26.5% d^6, and 2.8% d^7.